A numerical method based on the moving mesh for the solving of a mathematical model of the avascular tumor growth

Mina Bagherpoorfard
Department of Applied Mathematics,
Ferdowsi University of Mashhad, Mashhad, Iran.
E-mail: `mi.bagherpoorfard@stu-mail.um.ac.ir`

Ali Reza Soheili
Department of Applied Mathematics,
Ferdowsi University of Mashhad, Mashhad, Iran.
E-mail: `soheili@um.ac.ir`

Abstract   Using adaptive mesh methods is one of the strategies to improve numerical solutions in time-dependent partial differential equations. The moving mesh method is an adaptive mesh method, which, firstly does not need an increase in the number of mesh points, secondly reduces the concentration of points in the steady areas of the solutions that do not need a high degree of accuracy, and finally places the points in the areas, where a high degree of accuracy is needed.

In this paper, we improved the numerical solutions for a three-phase model of avascular tumor growth by using the moving mesh method. The physical formulation of this model uses reaction-diffusion dynamics with the mass conservation law and appears in the format of the nonlinear system of partial differential equations based on the continuous density of three proliferating, quiescent, and necrotic cell categorizations.

Our numerical results show more accurate numerical solutions, as compared to the corresponding fixed mesh method. Moreover, this method leads to the higher order of numerical convergence.

1. Introduction

Cancer is the second-leading cause of death on the global scale and deaths from cancer increased more than 17 percent between 2006 and 2016 [14, 30]. The accepted theory about the origin of cancerous cells emergence states that mutations occur in the key genes of a normal cell DNA and make it into a cancerous cell [50]. The factors causing these mutations are, to a great extent, unknown, yet they are composed of two general factors of inheritance and environment. On the one hand, the result of these mutations is an increase of cell proliferation rate; on the other hand, a reduction in cellular mortality leads to the formation of a mass of cancerous cells called tumor [33].

The growth process of a tumor consists of three distinct phases: avascular, angiogenesis, and metastatic. In the avascular phase, the tumor lacks blood vessels, feeds tumor cells and disposes of their waste materials, which are carried out through diffusion [11, 16]. Like normal cells, tumor cells supply their nutrients through the surrounding tissues by diffusion [40]. In the early stage of tumor growth, all of its cells receive sufficient nutrients and the tumor grows rapidly, yet with the passage of time and by an increase in the tumor size the amount of food is not sufficient. Therefore, this reduces the growth, the size of tumor reaches a saturated size and its growth nearly stops [26, 32, 58]. In case of tumor cells food shortage, they send signals to blood vessels near the tumor mass, which leads to the angiogenesis process [17]. During this process, the cell spatters a chemical composition named tumor angiogenic factor(TAF) in the surrounding tissues, thereby stimulating the neighboring blood vessels, drawing them toward the tumor, and finally penetrating into the tumor [25, 34]. As a result, tumor cells have access to the blood vessels which are considered as a rich food resource for cells, and the rapid growth of tumor begins again. For this reason, new treatments are oriented toward a condition in which tumor blood vessels are attacked. When the tumor is equipped with blood vessels, cells can enter blood circulation, travel to other parts of the body (travel to other healthy tissues and organs), inhabit other places, and create the secondary tumors. This phase of tumor growth is dangerous and lethal because the finding, detecting, and treating of tumors are difficult [52]. The avascular phase of tumor growth is intended in this paper. The tumors in avascular phase are rarely detectable due to their small size. Therefore, their clinical investigation is difficult, but their experimental investigation is easy through a multicellular spherical system [42, 58].

A multicellular spherical system consists of a spherical mass of cancerous cells which grow in a culture environment riched by enough and appropriate nutrients. The proven structure of multicellular spheres is made up of three areas. An outer area of living, proliferative, and fed cells, is a central inner area of dead cells where a strip of quiescent cells exists between these two areas. These quiescent cells are alive, yet they do not proliferate. They begin to proliferate as they receive enough nutrients again [27]. At the beginning, when the sphere size is small, all of the sphere cells will receive enough nutrients and the growth will begin at an exponential rate. By an increase in the sphere growth and the penetration of less nutrients into the inner cells, the areas of quiescent and dead cells are formed and the growth speed enters a linear phase. With the passage of more time and because of some of the intracellular causes, the growth of the sphere approximately will be stopped and lead to a sphere with a maximal size [3, 21, 26, 28, 31, 39, 58].

The oldest mathematical model of avascular tumor growth dates back to a model presented by Thomlinson and Gray [60]. Then, the model was developed by Burton [13] and Greenspan [31]. In the Greenspan model, cells inside an avascular tumor are divided into three distinct areas of proliferating, quiescent, and necrotic cells. The border among these three areas is determined by the surfaces of mitotic inhibitors and nutrients. Greenspan article opened a new way in the field of mathematical models of the avascular tumor growth, and numerous researchers followed and developed his work. As an instance, McElwain and Morris [49] obtained a similar behavior

as Greenspan model behavior; assuming that the only mechanism of cell loss was apoptosis. Chaplain, Benson, and Maini [19] applied a variable spatial diffusion coefficient which led to the same qualitative results as Greenspan model ones. Byrne and Chaplain [15] generalized the role of inhibitors in the Greenspan model, and they investigated the impact of cellular death mechanisms on the tumor growth distinctly. For other extensions of Greenspan model, see [24, 56, 2, 46, 47, 18].

Ward and King [62] and Sherratt and Chaplain [54] models are considered as an evolution of avascular tumor growth models. Unlike all previous models, a variety of cells within the tumor in distinct spaces is not assumed in these models; however, the models are presented continuously based on the density of all various cells and depend on the density of nutrients. Three proliferating, quiescent, and necrotic intratumoral cells categories are considered in the Sherratt and Chaplain model, while the Ward and King model is a biphasic model in which only proliferating and dead cells are considered and quiescent cells, considered as a proven part of the avascular tumor structure, are not in this model. In Ward and King model, a mechanism is not considered for the prevention of tumor growth. Therefore, they developed their model to achieve the saturated phase of the growth considering basic cellular material diffusion like protein, DNA, and fat [63]. This model was investigated by Slezaka et al. [57] numerically with a predictor-corrector pattern based on the finite difference method. In [9, 10, 59] the term related to the extracellular matrix has been added to the nonlinear system of Sherratt and Chaplain. Also, intracellular random changes have been made and discussed. Darbyshire [23] addressed the numerical solution of this model in parallel and used CUDA programming framework to parallelize the explicit finite difference method. Some other continuous models can be seen in [51, 61, 65, 47, 44]. Alongside the development of continuous models, there are still some of discrete models like Kiran, Jayachandran, and Lakshminarayanan in [41] that assumed distinct areas for tumor cells and searched for the geometrical place of borders between areas during the time by considering the amount of nutrients.

Roose, Chapman, and Maini [52] conducted a complete summarization of references for discrete and continuous models of avascular tumor growth. Moreover, we can refer to [11] for another review.

Adaptive mesh methods have been considered for numerical solutions to mathematical models of tumor growth in recent years [4, 5, 6, 7, 8, 22, 43, 64]. Lee et al. [43] applied the static moving mesh methods for a biphasic model provided by Breward [12], based on the water and cell. They presented three moving mesh methods based on the velocity, compared them and used the Euler explicit method or Runge–Kutta methods at each time step. Amoddeo [4, 5] presented a model for the investigation of the effects of oxygen shortage on the dynamic interaction of cancerous cells by the UPA system in the avascular phase and addressed the numerical solution of the model by using the moving finite element. Also, the density of cancerous cells is used as the leading agent of mesh points. In recent years, he implemented the MMPDE numerical technique based on the monitor function using a finite element discretization in space to solve the PDE systems arising from the mathematical modelling of cancer cell proliferation and growth [5, 6, 7, 8].

Adaptive mesh methods for time-dependent differential equations fall in static and

dynamic categories. In static methods, an initial mesh and the answer to it are evident in the beginning; hence, a new mesh which may contain different numbers of mesh points at each time step is constructed by various techniques. The answer is interpolated from the old mesh to the new mesh. Therefore, an approximate solution is defined for the new mesh [36, 37, 48].

In the dynamic methods which are known as moving mesh methods, a time-dependent equation is defined for mesh movement based on the equidistribution principle. In this method, without any change in the number of mesh points at each time step, at first the mesh movement equation and physical equations are coupled and then this system of equations is resolved simultaneously; after that physical answers and new mesh places are obtained.

In this technique, the movement of mesh points is led by a controller parameter which is calculated during the resolution process. Therefore, in areas where there are rapid variations of the answer and there is a need to refine the mesh for improving discrete answers, the points are more concentrated without an increase of the number of mesh points [35, 36, 37, 38, 48]. Therefore, using these methods compared to a uniform discretization based methods, can prevent extra computational fees besides the improvement of answers accuracy.

In this paper, we focus on a powerful model for avascular tumor growth, three-phase continuous, Sherratt and Chaplain model. This model is in the format of a system of nonlinear time-dependent partial differential equations. Numerical solutions for this model are improved by the moving mesh method. Results show that the numerical solutions based on the moving mesh method and fixed mesh method have a significant difference. Applying the moving mesh method yields highly accurate solutions, as well as the increasing the numerical convergence order.

2. **The Model**

Ward and King [62] and Sherratt and Chaplain [54] models are the first models to consider a discrete cellular space for an avascular tumor. There are two kinds of cell, living and dead ones, in the Ward and King model and the cellular movement has not been considered in the model. Therefore, tumor growth is only dependent on cell division.

Our desired model in this paper is the three-phase model introduced by Sherratt and Chaplain [54]. The continuous density of proliferating, quiescent, and necrotic cell categorizations has been used in this model, which have been shown as $p(x,t)$, $q(x,t)$, and $n(x,t)$, respectively. Moreover, unlike most models, in this model, the formulation structure has been considered as in vivo-oriented than in vitro-oriented. In this regard, the cells movement is considered as a factor of tumor growth beside cell division.

In a single cell population or multiple cell populations with an adequate intercellular space, the cell movement can be expressed by the approved model of linear diffusion. Moreover, a reaction-diffusion expression can be a good indicator of cellular movement for a single close-packed cellular population [20, 55]. However, in the close-packed cell populations where a variety of cells interact with one another, the diffusion model is not appropriate because using it means that the movement of a kind of cell is

independent of the presence of other kinds of cell and cellular populations can be combined with one another. This subject contradicts the contact inhibition of the migration phenomenon because the cells will stop as a consequence of making one kind of cell contact other kinds of cells based on this phenomenon [1].

In the Sherratt and Chaplain model, it is assumed that proliferating and quiescent cell populations have the same motility and the effect of contact inhibition is considered as well. Since cells move toward a direction where there is more space, the overall cellular flux is proportionate to the negative gradient of cellular density. Therefore, the two expressions, $-\frac{p}{p+q}\frac{\partial(p+q)}{\partial x}$ and $-\frac{q}{p+q}\frac{\partial(p+q)}{\partial x}$ are applied for contact inhibition features in this model [53]. Also, using mass conservation for the cells leads to the following system of partial differential equations:

$$\frac{\partial p}{\partial t} = \frac{\partial}{\partial x}\left(\frac{p}{p+q}\frac{\partial(p+q)}{\partial x}\right) + g(c)p(1-p-q-n) - f(c)p, \tag{2.1}$$

$$\frac{\partial q}{\partial t} = \frac{\partial}{\partial x}\left(\frac{q}{p+q}\frac{\partial(p+q)}{\partial x}\right) + f(c)p - h(c)q, \tag{2.2}$$

$$\frac{\partial n}{\partial t} = h(c)q. \tag{2.3}$$

$c(x,t)$ is the local nutrient concentration and has the below form

$$c = \frac{c_0\gamma}{\gamma + p}(1 - \alpha(p+q+n)) \tag{2.4}$$

where α and γ are dimensionless parameters.

$g(c)$ is the mitosis rate function of the proliferating cells and is an increasing function, proliferating cells become quiescent at the rate $f(c)$, and the rate of turning the quiescent cells to necrosis is denoted by $h(c)$. Both f and h are the decreasing functions and will be zero as c turns toward to $+\infty$; in addition $f(c) > h(c)$.

For the initial conditions, we have $p(x,0) = e^{-0.1x}$, $q(x,0) = 0$, $n(x,0) = 0$, and $c_0 = 1$. The boundary conditions are $\frac{\partial p}{\partial x} = 0$, $\frac{\partial q}{\partial x} = 0$, and $\frac{\partial c}{\partial x} = 0$, at $x = 0$ and $x = 210$. ($x = 210$ is chosen as a sufficiently large value.)

3. **The Numerical Method**

Equidistribution principle (EP) is the main idea in the moving mesh methods and plays the key role in obtaining the moving mesh partial differential equation (MMPDE) [37].

Suppose that $[a, b]$ is the physical domain with a physical variable x, and $[0, 1]$ is the computational domain for a computational variable ξ. A coordinates transformation between two domains is as follows:

$$\Omega_c = [0,1] \to \Omega = [a,b],$$
$$x = x(\xi, t), \qquad \xi \in [0,1],$$
$$x(0, t) = a, \qquad x(1, t) = b.$$

Let $\xi_i = \frac{i}{n}$, $i = 0, 1, \ldots, n$, be a uniform mesh on $[0,1]$, and let $a = x_0 < x_1 < \cdots < x_n = b$ be a corresponding mesh on physical domain, where $x_i = x(\xi_i, t)$, $i =$

$0, 1, \ldots, n$, is defined based on the EP; so that some measure of the solution error is equal at each subinterval [36].

We introduce a monitor function $M(x, t)$ which indicates some error measurement in the approximate solutions to the original PDE. The mesh in x is satisfied in the EP for all values of time t, which could be written down as

$$\int_a^{x(\xi,t)} M(\tilde{x}, t)d\tilde{x} = \xi\theta(t), \tag{3.1}$$

where

$$\theta(t) = \int_a^b M(\tilde{x}, t)d\tilde{x}.$$

By differentiating twice (3.1), it yields

$$\frac{\partial}{\partial \xi}\{M(x(\xi, t), t)\frac{\partial}{\partial \xi}x(\xi, t)\} = 0. \tag{3.2}$$

If a mesh is satisfied in (3.2) at the time $t + \tau$ ($0 < \tau << 1$) instead of t; we have

$$\frac{\partial}{\partial \xi}\{M(x(\xi, t + \tau), t + \tau)\frac{\partial}{\partial \xi}x(\xi, t + \tau)\} = 0, \tag{3.3}$$

where the parameter τ is called relaxation time.

Using the Taylor expansions for (3.3) after the dropping of higher order terms, we obtain

$$\frac{\partial}{\partial \xi}(M\frac{\partial \dot{x}}{\partial \xi}) + \frac{\partial}{\partial \xi}(\frac{\partial M}{\partial \xi}\dot{x}) = -\frac{\partial}{\partial \xi}(\frac{\partial M}{\partial t}\frac{\partial x}{\partial \xi}) - \frac{1}{\tau}\frac{\partial}{\partial \xi}(M\frac{\partial x}{\partial \xi}). \tag{MMPDE2}$$

For more MMPDEs see [29, 36, 37].

In our numerical results, we use

$$\frac{\partial x}{\partial t} = -\frac{1}{\tau}\frac{\partial}{\partial \xi}(M\frac{\partial x}{\partial \xi}). \tag{MMPDE5}$$

For accurate and efficient numerical solutions, we should design the suitable monitor functions. Common choices for the monitor function are the arc-length monitor function,

$$M = (1 + |u_x|^2)^{1/2}, \tag{3.4}$$

curvature monitor function,

$$M = (1 + |u_{xx}|^2)^{1/4}, \tag{3.5}$$

and optimal mesh monitor function,

$$M = (1 + \frac{1}{\alpha}|u_x|^2)^{1/3}, \qquad \alpha = \max\{1, (\frac{1}{b - a}\int_a^b |u_{xx}|^{2/3})^3\}. \tag{3.6}$$

The system of equations (2.1)–(2.3) in the computational coordinates are

$$\dot{p} - \frac{p_\xi}{x_\xi}\dot{x} = \frac{rp_\xi - pr_\xi}{(rx_\xi)^2}r_\xi + \frac{p}{rx_\xi}(\frac{r_\xi}{x_\xi})_\xi + g(c)p(1 - r - n) - f(c)p,$$

(3.7)

$$\dot{q} - \frac{q_\xi}{x_\xi}\dot{x} = \frac{rq_\xi - qr_\xi}{(rx_\xi)^2}r_\xi + \frac{q}{rx_\xi}(\frac{r_\xi}{x_\xi})_\xi + f(c)p - h(c)q,$$

(3.8)

$$\dot{n} - \frac{n_\xi}{x_\xi}\dot{x} = h(c)q,$$

(3.9)

where $r = p + q$.

We employ the method of lines approach for the equations (3.7)–(3.9). The partial derivatives with respect to the space variables are discretized by using central finite difference schemes. Therefore, a system of ODEs is obtained as follows:

$$\dot{p}_j - \frac{p_{j+1} - p_{j-1}}{x_{j+1} - x_{j-1}}\dot{x} = \frac{(p_{j+1} - p_{j-1})r_j(r_{j+1} - r_{j-1})}{r_j^2(x_{j+1} - x_{j-1})^2} - \frac{p_j(r_{j+1} - r_{j-1})^2}{r_j^2(x_{j+1} - x_{j-1})^2}$$
$$+ \frac{2p_j}{r_j(x_{j+1} - x_{j-1})}(\frac{r_{j+1} - r_j}{x_{j+1} - x_j} - \frac{r_j - r_{j-1}}{x_j - x_{j-1}})$$
$$+ g(c_j)p_j(1 - r_j - n_j) - f(c_j)p_j,$$

(3.10)

$$\dot{q}_j - \frac{q_{j+1} - q_{j-1}}{x_{j+1} - x_{j-1}}\dot{x} = \frac{(q_{j+1} - q_{j-1})r_j(r_{j+1} - r_{j-1})}{r_j^2(x_{j+1} - x_{j-1})^2} - \frac{q_j(r_{j+1} - r_{j-1})^2}{r_j^2(x_{j+1} - x_{j-1})^2}$$
$$+ \frac{2q_j}{r_j(x_{j+1} - x_{j-1})}(\frac{r_{j+1} - r_j}{x_{j+1} - x_j} - \frac{r_j - r_{j-1}}{x_j - x_{j-1}})$$
$$+ f(c_j)p_j - h(c_j)q_j,$$

(3.11)

$$\dot{n}_j - \frac{n_{j+1} - n_{j-1}}{x_{j+1} - x_{j-1}}\dot{x} = h(c_j)q_j,$$

(3.12)

where the "dot" refers to the time, $x_j = x(\xi_j, t)$, and $p_j = p(x(\xi_j, t), t), j = 1, \ldots, N - 1$, also similarly for q and n. We use

$$c_j = \frac{c_0\gamma}{\gamma + p_j}(1 - \alpha(r_j + n_j)),$$

where $c_j = c(x(\xi_j, t), t), j = 1, \ldots, N - 1$, as the discretization form of (2.4). Moreover, the semi-discretization of (MMPDE5) can be given by

$$\dot{x}_j = \frac{1}{\tau}(\frac{M_{j+1} + M_j}{2\Delta\xi^2}(x_{j+1} - x_j) - \frac{M_j + M_{j-1}}{2\Delta\xi^2}(x_j - x_{j-1})),$$

(3.13)

in which the boundary conditions are

$$\dot{x}_0 = \dot{x}_N = 0.$$

We couple the equations (3.10)–(3.12) and (3.13). Then, a system involves $(4N - 4)$ ordinary differential equations for $p_j(t), q_j(t), n_j(t),$ and $x_j(t), j = 1, \ldots, N - 1$, is constituted. We use the MATLAB ODE solver (ode15s) to integrate the resulting system.

Here, we can use the monitor functions such as the semi-arc-length monitor function

$$M = (1 + \frac{\beta_1 |p_x|^2 + \beta_2 |q_x|^2 + \beta_3 |n_x|^2}{\beta_1 + \beta_2 + \beta_3})^{1/2}, \tag{3.14}$$

semi-curvature monitor function

$$M = (1 + \frac{\beta_1 |p_{xx}|^2 + \beta_2 |q_{xx}|^2 + \beta_3 |n_{xx}|^2}{\beta_1 + \beta_2 + \beta_3})^{1/2}, \tag{3.15}$$

and

$$M = \frac{\beta_1 M_1 + \beta_2 M_2 + \beta_3 M_3}{\beta_1 + \beta_2 + \beta_3}, \tag{3.16}$$

where M_1, M_2, and M_3 can be any of the monitor functions (3.4)–(3.6) based on p, q, and n, respectively. For example,

$$M_1 = (1 + |p_x|^2)^{1/2},$$
$$M_2 = (1 + |q_x|^2)^{1/2},$$
$$M_3 = (1 + |n_x|^2)^{1/2}.$$

However, in (3.14)–(3.16)

$$\beta_1 + \beta_2 + \beta_3 = 1.$$

In our numerical experiments, semi-arc-length monitor function (3.14) have been used.

4. **Results and Discussion**

In this section, we will address the resolution of the avascular tumor growth model by the method presented in the section 3. Model parameters have been considered as follows: [54]

$$f(c) = (1 - tanh(4c - 2))/2,$$
$$h(c) = f(c)/2,$$
$$g(c) = \beta e^{\beta c},$$
$$\alpha = 0.8, \beta = 0.5, \ and \ \gamma = 10.$$

These functions have introduced in section 2. The density of the proliferating, quiescent, and necrotic cells in $t = 0, 2, \ldots, 16$ weeks has been shown as $p(x)$, $q(x)$, and $n(x)$ in Figures $1-3$, respectively. The investigation of these diagrams indicates that the proliferating cells will be extended by the proliferation over time and move toward the outer edge of the tumor, which leads to an increase in tumor size and correspondingly the quiescent group cells are formed and extend beyond the proliferated cells. Necrotic group cells which are concentrated in a small area around the center of the tumor at the initial times of tumor growth will occupy a wider area around the center

of the tumor with the passage of time, while their density toward the center of the tumor is increasing.
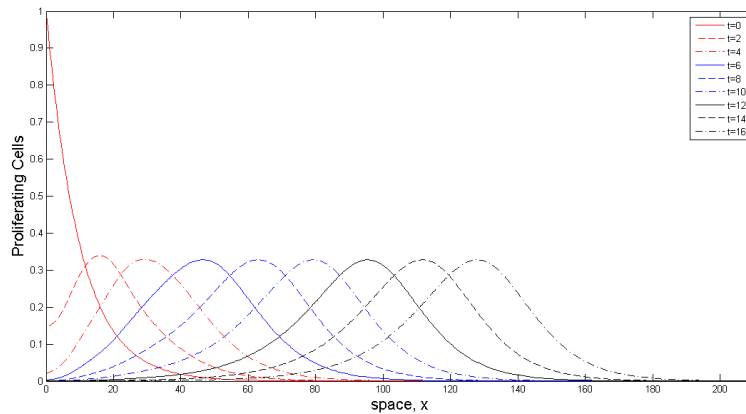
FIGURE 1. *Proliferating cells density plotted as a function of space at times $t = 0, 2, \ldots, 16$. Curves move from left to right as time increases.*
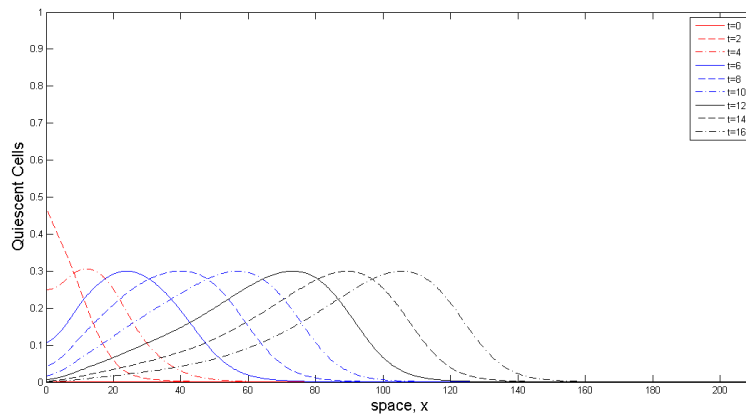
FIGURE 2. *Quiescent cells density plotted as a function of space at times $t = 0, 2, \ldots, 16$. Curves move from left to right as time increases.*

This model is based on the continuous density of these three group cells, and the artificial assumption of distinct cell areas has not been considered. However, the investigation of the geometric place of these three cells categorizations in every
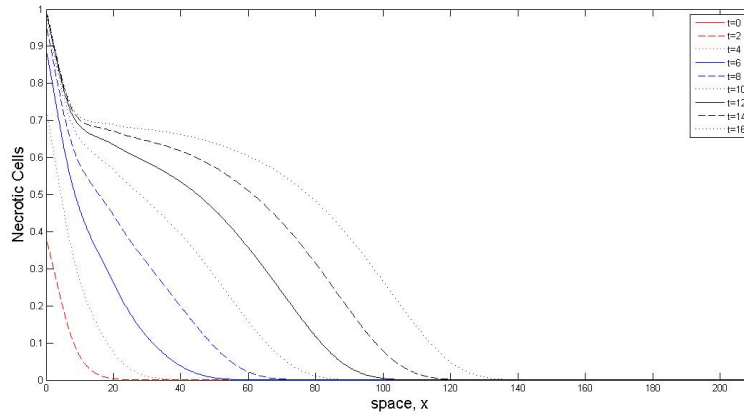
FIGURE 3. *Necrotic cells density plotted as a function of space at times $t = 0, 2, \ldots, 16$. Curves move from left to right as time increases.*

constant time shows that the main population of cells of the proliferating group cells is in the location of the tumor outer layer, where the density of these cells is much more than that of necrotic and quiescent cells. Most of the necrotic group cells are concentrated in an area adjacent to the tumor center. In this area, the density of the two other cells categorizations is negligible and particularly when they approach the center of tumor, their density becomes approximately zero. While, the density of necrotic cells increases by approaching the tumor center. The area of the quiescent cells concentration is a strip which is placed between the concentration areas of the two other cell categorizations. In Figure 4, the concentration areas of these three cell categorizations have been shown in $t = 16$ time.

To obtain an estimation of the method error and investigate its numerical convergence, we resolved the model for $t \in [0, 4]$ and for different N cells with the moving mesh and fixed mesh methods($N = 150, 200, 300, 400, 600$). We consider the point-to-point error based on each of the L_2, L_1, and L_∞ norms, respectively, as follows, and we expected these errors to be reduced by an increase in N:

$$
E_{L_2}(U_N^T) = \left[\sum_{i=1}^{k} \left(U_{N_R}^T (X_i) - U_N^T (X_i) \right)^2 \right]^{\frac{1}{2}},
$$

$$
E_{L_1}(U_N^T) = \sum_{i=1}^{k} |U_{N_R}^T (X_i) - U_N^T (X_i)|,
$$

$$
E_{L_\infty}(U_N^T) = Max_{i=1,\ldots,k} |U_{N_R}^T (X_i) - U_N^T (X_i)|.
$$
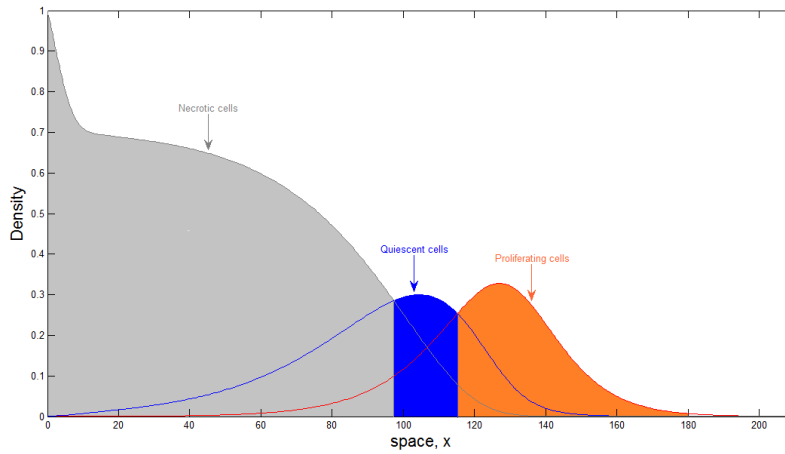
FIGURE 4.   *Concentration areas of proliferating, quiescent, and necrotic cells.*

Where U^T can be each of the p, q, and n cells in the time $t = T$; N_R is the number of reference mesh points, which is considered as $N_R = 800$, and X_i, $i = l, \ldots, k$, are the specified points of the physical domain. In the moving mesh method, U^T values in X_i, $i = l, \ldots, k$, should be calculated by interpolation.

Given $E\left(U_N^T\right) \simeq \eta\left(\dfrac{1}{N}\right)^{\alpha}$, which works for sufficiently large N's, an estimation of convergence order can be obtained by the following equation:

$$\alpha_{U,N} = -\log_2\left(\frac{E(U_{2N})}{E(U_N)}\right).$$

The results related to the calculation of error based on L_∞ norm in $T = 4$ and for $k = 20$ equal-distance points from the physical domain and an estimation of convergence order of both methods (the moving mesh and fixed mesh methods) have been presented in Table 1. In this table, it can be seen that in both methods, an increase in N reduces the error, but the moving mesh method enjoys a higher order of convergence, as compared to the fixed mesh. Moreover, the error diagrams for p, q, and n have been drawn as a function of N based on each of the three L_2, L_1, and L_∞ norms for $T = 4$ in Figures 5−7.

The tumor growth stages in the avascular phase are in such a manner that in the beginning, the proliferating cells grow regularly and exponentially due to the adequacy of nutrients. As the time proceeds, the tumor growth becomes linear due to the inadequacy of nutrients and the growth of proliferating cells and finally stops because of some intracellular activities. We have investigated this process for our numerical results. In Figure 8, the growth diagram of proliferative cells has been drawn as a function of time for $t \in [0, 18]$, and the above-mentioned growth process is completely

TABLE 1. Error estimation for p, q, and n with order of convergence.

$Method$	N	$E_{L_\infty}(p_N)$	$\alpha_{p,N}$	$E_{L_\infty}(q_N)$	$\alpha_{q,N}$	$E_{L_\infty}(n_N)$	$\alpha_{n,N}$
Fixed Mesh	150	2.544×10^{-3}	-	3.084×10^{-3}	-	2.460×10^{-2}	-
	200	1.911×10^{-3}	-	2.351×10^{-3}	-	1.813×10^{-2}	-
	300	1.151×10^{-3}	1.14	1.428×10^{-3}	1.11	1.071×10^{-2}	1.19
	400	7.193×10^{-4}	1.41	8.936×10^{-4}	1.39	6.621×10^{-3}	1.45
	600	2.495×10^{-4}	1.20	3.101×10^{-4}	1.20	2.272×10^{-3}	1.23
Moving Mesh	150	3.772×10^{-6}	-	4.164×10^{-6}	-	3.625×10^{-6}	-
	200	1.926×10^{-6}	-	2.278×10^{-6}	-	1.927×10^{-6}	-
	300	7.486×10^{-7}	2.33	9.366×10^{-7}	2.15	7.830×10^{-7}	2.21
	400	3.950×10^{-7}	2.28	4.600×10^{-7}	2.30	3.867×10^{-7}	2.31
	600	4.296×10^{-8}	2.12	1.138×10^{-7}	2.04	7.711×10^{-8}	2.34
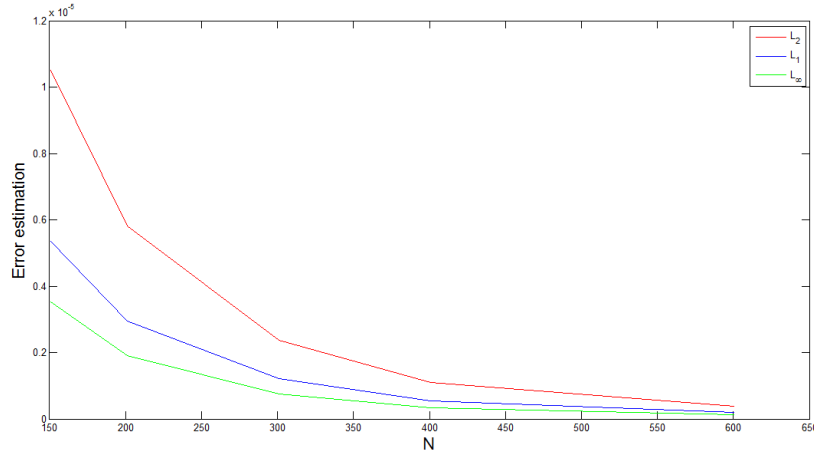
FIGURE 5. *Error estimation by L_2, L_1, and L_∞ for p in $T = 4$.*

visible in this diagram.

In the moving mesh related diagrams, we have used the semi-arc-length monitor function (3.14) and four categories of $\{\beta_1, \beta_2, \beta_3\}$. Mesh trajectories have been shown in Figures $9-12$ for $t = 0$ to $t = 14$. In Figure 9, $\beta_1 = 1$ and $\beta_2 = \beta_3 = 0$. The effect of n and q cells density changes was removed from the mesh movement with this choice. As seen in this Figure, the concentration of mesh points during the time matches with an area which has the highest amount of p density. By putting $\beta_1 = \beta_2 = 0$ and $\beta_3 = 1$, the effect of narcotic cell density changes is dominated. The mesh trajectory corresponding to this state has been shown in Figure 10, where the concentration of points in all points is in an area around the center of the tumor which is widened over time. $\beta_1 = \beta_3 = 0$ and $\beta_2 = 1$ have been considered in Figure 11 In this state like the two previous states, the movement of mesh points is well coordinated with quiescent cell density changes in the course of time. To improve the calculations of every three
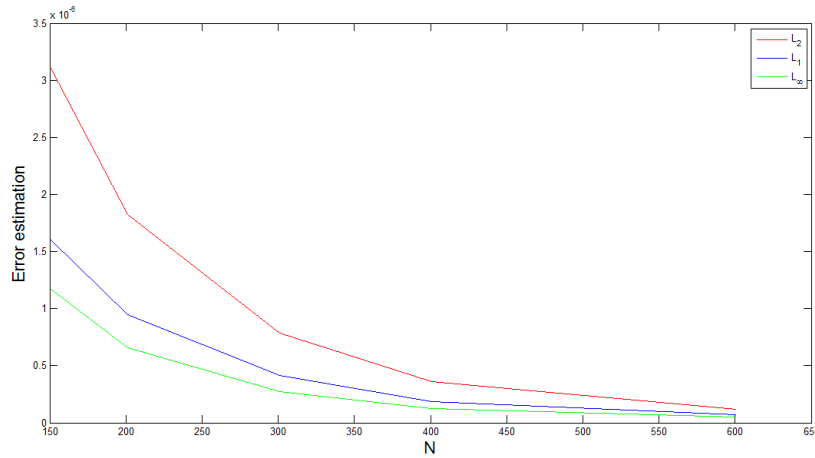
FIGURE 6. *Error estimation by L_2, L_1, and L_∞ for q in $T = 4$.*
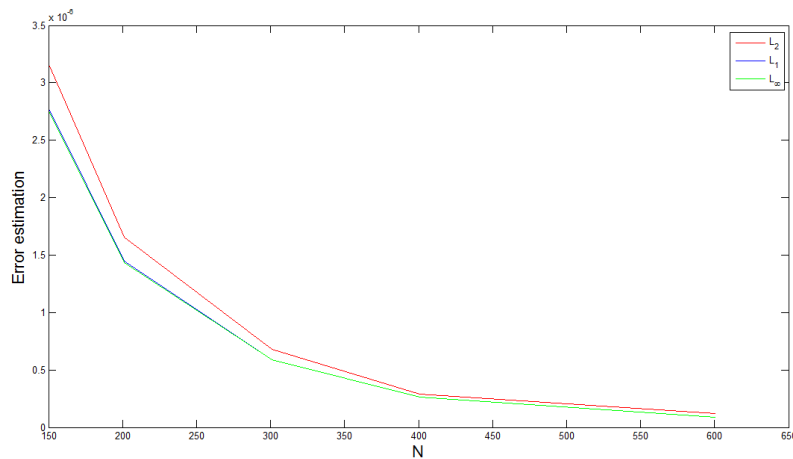
FIGURE 7. *Error estimation by L_2, L_1, and L_∞ for n in $T = 4$.*

proliferating, quiescent, and necrotic resolution categorizations, $\beta_1 = \beta_2 = \beta_3 = \dfrac{1}{3}$ can be placed, which leads to the distribution of points in line with the density changes of all the three cells categorizations (Figure 12).

The last part of this section is dedicated to the obtained numerical results of nutrients density, $C(x, t)$. The density of nutrients in tumor for $t = 0, 2, \ldots, 14$, as a function of the place has been drawn in Figure 13. These diagrams suggest that at all time a high amount of nutrients is available for the cells outer layer and a lower amount
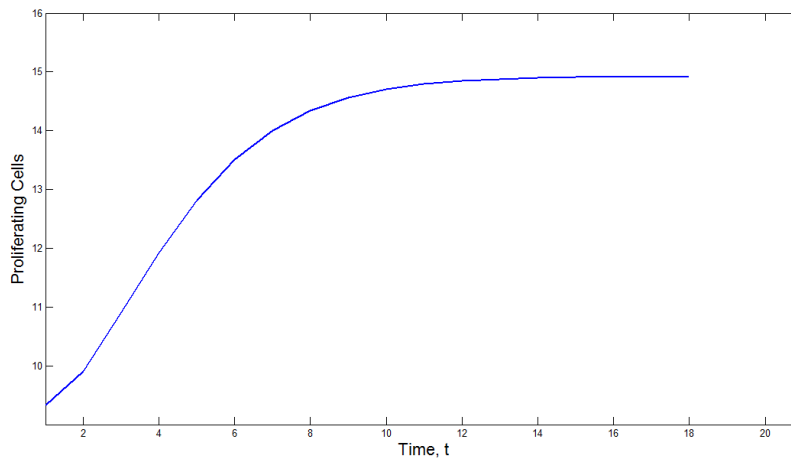
FIGURE 8. *Growth process of proliferating cells as a function of time*
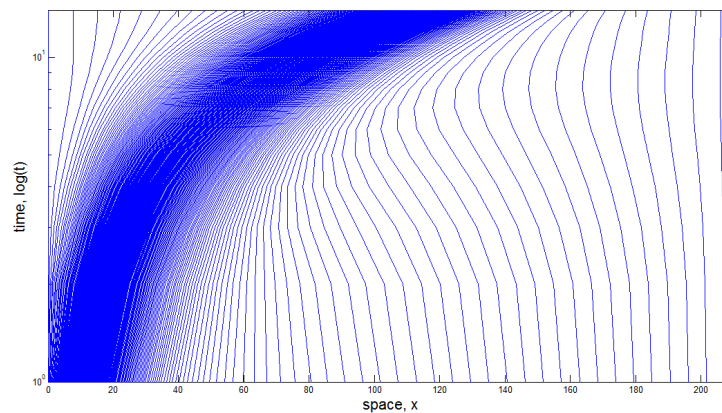
FIGURE 9. *Mesh trajectories with $\beta_1 = 1$ and $\beta_2 = \beta_3 = 0$.*

of them is available for cells surrounding the tumor center. Moreover, the passage of time and the increase of tumor size cause the reduction of nutrients which go to the inner cells, particularly the cells surrounding the tumor center. This distribution of density is well accepted, because cells receive nutrients from the surrounding tissues through diffusion in the avascular phase of tumor growth. Given the restriction of these nutrients, when the tumor becomes larger, less nutrients will go to the central cells.

We became interested in investigating mesh trajectories based on $C(x, t)$. In this regard, we have obtained mesh trajectories for $t \in [0, 14]$ using (3.4) whose results can
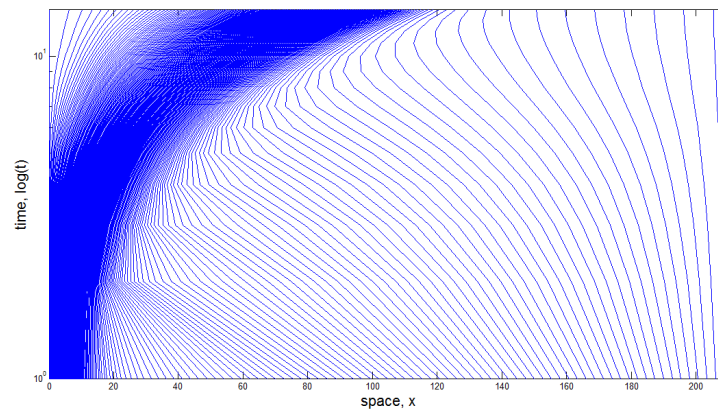
FIGURE 10. *Mesh trajectories with $\beta_2 = 1$ and $\beta_1 = \beta_3 = 0$.*
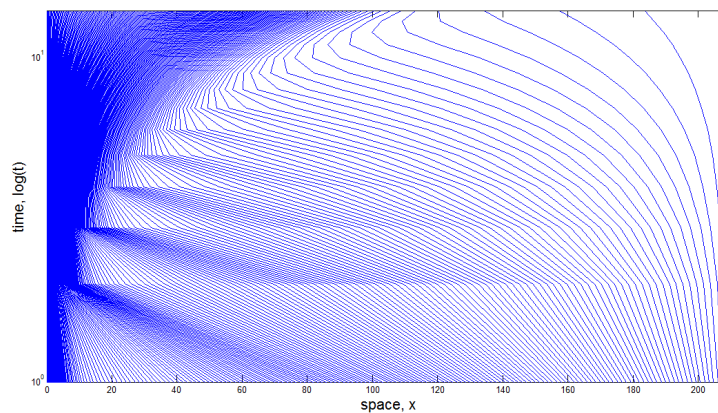
FIGURE 11. *Mesh trajectories with $\beta_3 = 1$ and $\beta_1 = \beta_2 = 0$.*

be seen in Figure 14. The concentration of mesh points during the time is proportional to $C(x, t)$ and changes toward the outer layer of tumor.

5. **Conclusion**

Because of the subject nature, the numerical results of mathematical models related to the cancer process, such as different tumor growth phases, drugs influence processes, various treatments on cancerous cells, and other similar models enjoy a substantial sensitivity. Therefore, it is essential to develop the numerical solution to these models using methods and techniques whith high accuracy and performance.
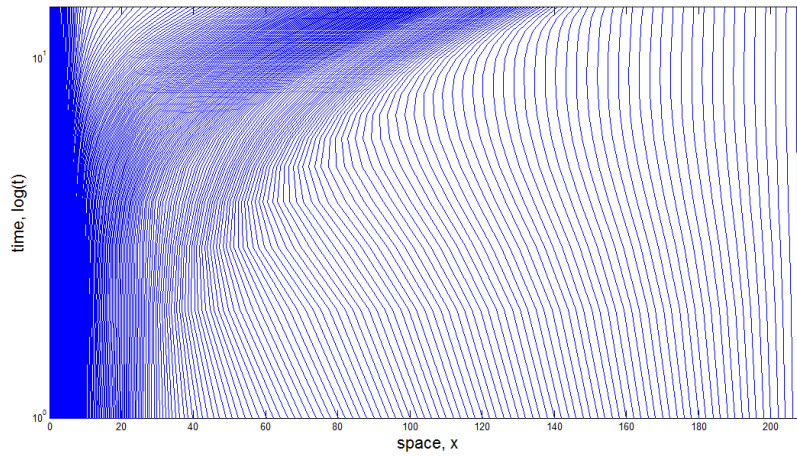
FIGURE 12. *Mesh trajectories with $\beta_1 = \beta_2 = \beta_3 = \frac{1}{3}$.*
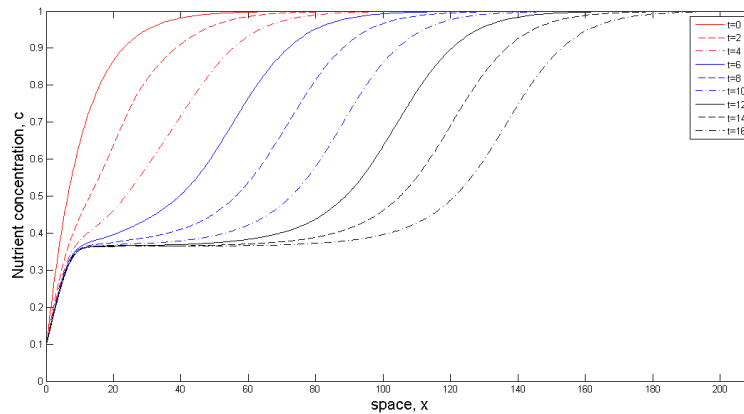
FIGURE 13. *Nutrients concentration plotted as a function of space at times $t = 0, 2, \ldots, 16$. Curves move from left to right as time increases.*

The avascular phase is the vital stage of tumor growth. Drug therapy and stopping the proliferation of cancer cells at this stage, before angiogenesis process, will prevent progression of the disease. The mathematical simulations of this phase are used to predict the size of primary tumor by passing the time, the rate of increasing the tumor radius, the tumor growth saturationthe time and beginning the angiogenesis process, the size of the necrotic core, and etc.

Among the existing models, the model under study in this paper has realistic features.
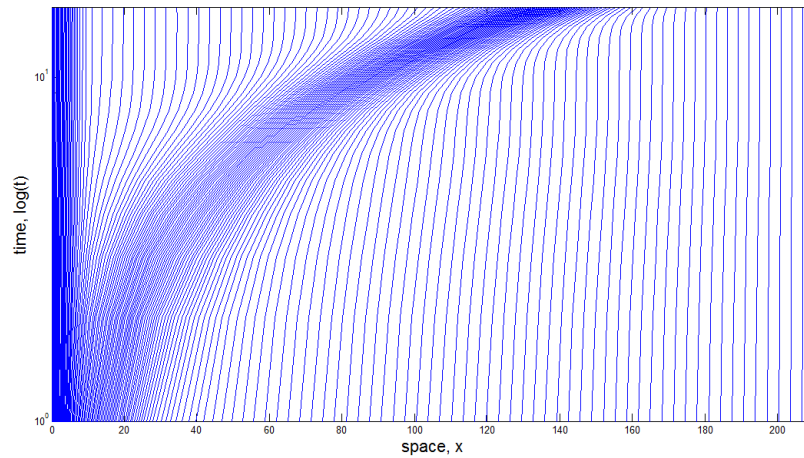
FIGURE 14. *Mesh trajectories based on the nutrients concentrations for $t \in [0, 14]$.*

For example, unlike other models, the model formulation has been directed towards in vivo instead of in vitro; the cells movement and cell division are considered as tumor growth factors; the real contact inhibition of the migration phenomenon is included in the model, separate intercellular space is not considered and the continuous cell density assumption is used, etc.

In this paper, we have numerically resolved the mentioned continuous three-phase avascular tumor growth model by means of a dynamic moving mesh method. This model is on the basis of the continuous density of three proliferating, quiescent, and necrotic cell groups that are dependent on the concentration of nutrients.

In the dynamic moving mesh method, using the equidistribution principle and the monitor function leads to the moving mesh partial differential equation (MMPDE) for the mesh points continuous movement during the time. We coupled MMPDE with the model physical system and obtained the approximate solutions to the model parameters and the position of mesh points at each time step simultaneously using the MOL. Our numerical results indicate that as compared to the fixed mesh, using the moving mesh method increases the order of numerical convergence, as well as being a good indicator of the avascular tumor growth process from the beginning to the time when it reaches the growth saturated state.

The monitor function is one of the important factors in this method which leads the mesh points toward the areas which need high accuracy. We defined the monitor functions based on the density changes of p, q, and n with the impact coefficients of β_1, β_2, and β_3 and drew mesh trajectories diagrams for different amounts of these parameters. However, the movement of mesh points and the area in which the points are concentrated are well-conformed with the physical behavior of these three cell categories in the tumor. Moreover, the process of mesh movement is justifiable based on the density of nutrients and the access of the tumor structure to these nutrients.

First of fall, this method increases the accuracy of numerical solutions. Secondly, it does not impose calculation costs for the increasing of the number of mesh points in order to enhance the accuracy. Therefore, it can be used in all fields for the purpose of developing a numerical solution to the models which need adequate accuracy.

References

1. M. Abercrombie, *Contact inhibition in tissue culture*, In vitro, *6*(2) (1970), 128–142.
2. J. A. Adam, *A simplified mathematical model of tumor growth*, Math. Biosci., *81*(2) (1986), 229–244.
3. J. A. Adam, and S. A. Maggelakis, *Diffusion regulated growth characteristics of a spherical prevascular carcinoma*, Bull. Math. Biol., *52*(4) (1990), 549–582.
4. A. Amoddeo, *Moving mesh partial differential equations modelling to describe oxygen induced effects on avascular tumour growth*, Cogent Phys., *2*(1) (2015), 1050080.
5. A. Amoddeo, *Oxygen induced effects on avascular tumour growth: a preliminary simulation using an adaptive grid algorithm*, J. Phys. Conf. Ser.,*633*(1) (2015), 012088.
6. A. Amoddeo, *Adaptive grid modelling for cancer cells in the early stage of invasion*, Comput. Math. Appl., *69* (2015), 610-619.
7. A. Amoddeo, *A moving mesh study for diffusion induced effects in avascular tumour growth*, Comput. Math. Appl., *75*(7) (2018), 2508-2519.
8. A. Amoddeo, *Modeling avascular tumor growth: Approach with an adaptive grid numerical technique*, J. Multiscale Model., *9*(03) (2018), 1840002.
9. K. C. Ang, *Analysis of a tumour growth model with MATLAB: Invited Paper*, 14th ATCM Conf. Proc., (2009).
10. K. C. Ang and L. S. Tan, *An avascular tumour growth model with random variation*, 8th ATCM Conf. Proc., *1* (2003), 153–161.
11. R. P. Araujo and D. S. McElwain, *A history of the study of solid tumour growth: the contribution of mathematical modelling*, Bull. Math. Biol., *66*(5) (2004), 1039–1091.
12. C. J. Breward, H. M. Byrne, and C. E. Lewis, *The role of cell-cell interactions in a two-phase model for avascular tumour growth*, G. Math. Biol., *45*(2) (2002), 125–152.
13. A. C. Burton, *Rate of growth of solid tumours as a problem of diffusion*, Growth, *30*(2) (1966), 157–176.
14. H. M. Byrne, *Using mathematics to study solid tumour growth*, In Proceedings of the 9th General Meetings of European Women in Mathematics, (1999), 81–107.
15. H. M. Byrne and M. A. J. Chaplain, *Growth of necrotic tumors in the presence and absence of inhibitors*, Math. Biosci., *135*(2) (1996), 187–216.
16. H. M. Byrne, T. Alarcon, M. R. Owen, S. D. Webb, and P. K. Maini, *Modelling aspects of cancer dynamics: a review. Philos*, Trans. A Math. Phys. Eng. Sci., *364*(1843) (2006), 1563–1578.
17. P. Carmeliet and R. K. Jain, *Angiogenesis in cancer and other diseases*, Nature *407*(6801) (2000), 249–257.
18. M. A. Chaplain and N. F. Britton, *On the concentration profile of a growth inhibitory factor in multicell spheroids*, Math. Biosci., *115*(2) (1993), 233–243.
19. M. A. Chaplain, D. L. Benson, and P. K. Maini, *Nonlinear diffusion of a growth inhibitory factor in multicell spheroids*, Math. Biosci., *121*(1) (1994), 1–13.
20. M. A. Chaplain and A. M. Stuart, *A model mechanism for the chemotactic response of endothelial cells to tumour angiogenesis factor*, Math. Med. Biol., *10*(3) (1993), 149–168.
21. A. D. Conger and M. C. Ziskin, *Growth of mammalian multicellular tumor spheroids*, Cancer Res., *43*(2) (1983), 556–560.
22. V. Cristini, X. Li, J. S. Lowengrub, and S. M. Wise, *Nonlinear simulations of solid tumor growth using a mixture model: invasion and branching*, J. Math. Biol., *58*(4) (2009), 723–763.

23. P. M. Darbyshire, *A system of coupled nonlinear partial differential equations describing avascular tumour growth are solved numerically using parallel programming to assess computational speedup*, Comput. Biol. Bioinform., *3*(5) (2015), 65–73.

24. A. S. Deakin, *Model for the growth of a solid in vitro tumor*, Growth, *39*(1) (1975), 159–165.

25. J. Folkman, *Graphs with monochromatic complete subgraphs in every edge coloring*, SIAM J. Appl. Math., *18*(1) (1970), 19–24.

26. J. Folkman and M. Hochberg, *Self-regulation of growth in three dimensions*, J. Exp. Med., *138*(4) (1973), 745–753.

27. J. P. Freyer and P. L. Schor, *Regrowth of cells from multicell tumor spheroids*, In Cell and Tissue Kinetics, *20*(2) (1987), 249–249.

28. J. P. Freyer and R. M. Sutherland, *Regulation of growth saturation and development of necrosis in EMT6/Ro multicellular spheroids by the glucose and oxygen supply*, Cancer Res., *46*(7) (1986), 3504–3512.

29. Q. Gao and S. Zhang, *Moving mesh strategies of adaptive methods for solving nonlinear partial differential equations*, Algorithms, *9*(4) (2016), 86.

30. Global Burden of Disease Collaborators, et al.,*Measuring progress and projecting attainment on the basis of past trends of the health-related sustainable development goals in 188 countries*, Lancet, *390* (2017), 1423–1459.

31. H. P. Greenspan, *Models for the growth of a solid tumor by diffusion*, Stud. Appl. Math., *51*(4) (1972), 317–340.

32. M. Haji-Karim and J. Carisson, *Proliferation and viability in cellular spheroids of human origin*, Cancer Res., *38*(5) (1978), 1457–1464.

33. D. Hanahan and R. A. Weinberg, *The hallmarks of cancer*, Cell, *100*(1) (2000), 57–70.

34. T. D. Henry, *Therapeutic angiogenesis*, British Medical J., *318*(7197) (1999), 1536–1539.

35. W. Huang and R. D. Russell, *Analysis of moving mesh partial differential equations with spatial smoothing*, SIAM J. Numer. Anal., *34*(3) (1997), 1106–1126.

36. W. Huang and R. D. Russell, *Adaptive moving mesh methods*, Volume 174 of Applied Mathematical Sciences, Springer New York, New York, 2011.

37. W. Huang Y. Ren, and R. D. Russell, *Moving mesh partial differential equations (MMPDES) based on the equidistribution principle*, SIAM J. Numer. Anal., *31*(3) (1994), 709–730.

38. J. M. Hyman, S. Li, and L. R. Petzold, *An adaptive moving mesh method with static rezoning for partial differential equations*, Comput. Math. Appl., *46*(10-11) (2003), 1511–1524.

39. W. R. Inch, J. A. McCredie, and R. M. Sutherland, *Growth of nodular carcinomas in rodents compared with multi-cell spheroids in tissue culture*, Growth, *34*(3) (1970), 271–282.

40. Y. Jiang, J. Pjesivac-Grbovic, C. Cantrell, and J. P. Freyer, *A multiscale model for avascular tumor growth*, Biophys. J., *89*(6) (2005), 3884–3894.

41. K. L. Kiran, D. Jayachandran, and S. Lakshminarayanan, *Mathematical modelling of avascular tumour growth based on diffusion of nutrients and its validation*, Can. J. Chem. Eng., *87*(5) (2009), 732–740.

42. L. A. Kunz-Schughart, M. Kreutz, and R. Knuechel, *Multicellular spheroids: a three-dimensional in vitro culture system to study tumour biology*, Int. J. Exp. Pathol., *79*(1) (1998), 1–23.

43. T. E. Lee, M. J. Baines, S. Langdon, and M. J. Tindall, *A moving mesh approach for modelling avascular tumour growth*, Appl. Numer. Math., *72* (2013), 99–114.

44. H. G. Lee,Y. Kim, and J. Kim, *Mathematical model and its fast numerical method for the tumor growth*, Math. Biosci. Eng., *12*(6) (2015), 1173–1187.

45. S. A. Maggelakis, *Effects of non-uniform inhibitor production on the growth of cancer cell cultures*, Appl. Math. Lett., *5*(5) (1992), 11–14.

46. S. A. Maggelakis and J. A. Adam, *Mathematical model of prevascular growth of a spherical carcinoma*, Math. Comput. Model., *13*(5) (1990), 23–38.

47. M. S. Mahmood, S. Mahmood, and D. Dobrota, *A numerical algorithm for avascular tumor growth model*, Math. Comput. Simul., *80*(6) (2010), 1269–1277.

48. R. Marlow, M. E. Hubbard, and P. K. Jimack, *Moving mesh methods for solving parabolic partial differential equations*, Comput. Fluids., *46*(1) (2011), 353–361.

49. D. L. S. McElwain and L. E. Morris, *Apoptosis as a volume loss mechanism in mathematical models of solid tumor growth*, Math. Biosci., *39*(1) (1978), 147–157.

50. F. Michor, Y. Iwasa, and M. A. Nowak, *Dynamics of cancer progression*, Nat. Rev. Cancer., *4*(3) (2004), 197–205.

51. G. J. Pettet, C. P. Please, M. J. Tindall, and D. L. S. McElwain, *The migration of cells in multicell tumor spheroids*, Bull. Math. Biol., *63*(2) (2001), 231–257.

52. T. Roose, S. j. Chapman, and P. K. Maini, *Mathematical models of avascular tumor growth*, Siam Rev., *49*(2) (2007), 179–208.

53. J. A. Sherratt, *Wave front propagation in a competition equation with a new motility term modelling contact inhibition between cell populations*, Proc. R. Soc. Lond., *456* (2000), 2365–2386.

54. J. A. Sherratt and M. A. Chaplain, *A new mathematical model for avascular tumour growth*, J. Math. Biol., *43*(4) (2001), 291–312.

55. J. A. Sherratt and J. D. Murray, *Models of epidermal wound healing*, Proc. R. Soc. Lond. Biol. Sci., *241*(1300) (1990), 29–36.

56. R. M. Shymko and L. Glass, *Cellular and geometric control of tissue growth and mitotic instability*, J. Theor. Biol., *63*(2) (1976), 355–374.

57. D. F. Slezaka, A. Sobaa, C. Sureza, M. Riska, and G. Marshalla, *Nonlinear pde system as model of avascular tumor growth*, Mecnica Computacional, *26* (2007), 1788–1799.

58. R. M. Sutherland, *Cell and environment interactions in tumor microregions: the multicell spheroid model*, Science *240*(4849) (1988), 177–184.

59. L. S. Tan and K. C. Ang, *A numerical simulation of avascular tumour growth*, ANZIAM J., *46* (2005), C902–C917.

60. R. H. Thomlinson and L. H. Gray, *The histological structure of some human lung cancers and the possible implications for radiotherapy*, Br. J. Cancer, *9*(4) (1995), 539–549.

61. M. J. Tindall and C. P. Please, *Modelling the cell cycle and cell movement in multicellular tumour spheroids*, Bull. Math. Biol., *69*(4) (2007), 1147–1165.

62. J. P. Ward and J. R. King, *Mathematical modelling of avascular-tumour growth*, Math. Med. Biol., *14*(1) (1997), 39–69.

63. J. P. Ward and J. R. King, *Mathematical modelling of avascular-tumour growth II: modelling growth saturation*, Math. Med. Biol., *16*(2) (1999), 171–211.

64. S. M. Wise, J. S. Lowengrub, and V. Cristini, *An adaptive multigrid algorithm for simulating solid tumor growth using mixture models*, Math. Comput. Model., *53*(1) (2011), 1–20.

65. S. M. Wise, J. S. Lowengrub, H. B. Frieboes, and V. Cristini, *Three-dimensional multispecies nonlinear tumor growth–I: model and numerical method*, J. Theor. Biol., *253*(3) (2008), 524–543.